JOURNAL OF Materials CHEMISTRY

Morphology, structure and growth of WS_2 nanotubes

Y. Q. Zhu,[a] W. K. Hsu,[a] H. Terrones,[a,b] N. Grobert,[a] B. H. Chang,[a] M. Terrones,[a,b] B. Q. Wei,[c] H. W. Kroto,[a] D. R. M. Walton,*[a] C. B. Boothroyd,[d] I. Kinloch,[d] G. Z. Chen,[d] A. H. Windle[d] and D. J. Fray[d]

[a]*School of Chemistry, Physics and Environmental Sciences, University of Sussex, Brighton, UK BN1 9QJ*
[b]*Instituto de Fisica, UNAM, Ap 1-1010, 76000 Queretaro, Mexico*
[c]*Department of Mechanical Engineering, Tsinghua University, Beijing 100084, P.R. China*
[d]*Department of Materials Science and Metallurgy, University of Cambridge, Pembroke Street, Cambridge, UK CB2 3QZ*

Received 2nd June 2000, Accepted 17th August 2000
First published as an Advance Article on the web 21st September 2000

The morphological and structural features of WS_2 nanotubes, generated from WO_x ($x \cong 2.7$) needles, by an *in-situ* heating process, have been studied by electron microscopy and X-ray diffraction (XRD), in conjunction with computer simulation. The results show that these inorganic fullerene nanotubes exhibit interesting differences when compared with carbon nanotubes (CNTs). In some cases the tube tips or segments are open. Occasionally the tube walls may be uneven. The sulfur distribution within the tubes is uniform, except for the edge layers which appear to contain less sulfur. Defects are often observed, particularly in the outer shells, which may be due to defective encapsulated WO_x phases. Octagonal and square-like defects appear to be associated with the closure of tube caps. Electron diffraction (ED) reveals that nearly half of the non-helical WS_2 nanotubes are of the armchair-type. A mechanism has been proposed to account for the extended inorganic nanotube growth.

1. Introduction

Nanometer-scale materials have attracted sustained interest following the discovery (1991), by Iijima, of carbon nanotubes formed from graphite.[1] Their structural features, associated growth mechanisms, physical and chemical properties have been comprehensively studied and various production methods have been developed,[2–5] some of which have been particularly successful in controlling growth. As a result, aligned CNTs and nanotube bundles, with desired diameters and lengths, have been fabricated.[6–9] Novel nanotubes, in which heteroatoms replace carbon, have been reported recently, *e.g.* BN,[10] $B_xC_yN_z$,[11,12] VO_x,[13] TiO_2,[14] and SiO_2.[15] Studies of the so-called Inorganic Fullerenes (IFs) MX_2 (M = W, Mo; X = S, Se) were pioneered by Tenne *et al.*[16–18] Because IF nanotubes are structurally similar to CNTs (*i.e.* they are composed of concentric cylinders),[1] the methods used to study CNTs are applicable. Here also, however, dichalcogenide MX_2 sheets differ from graphite in that they contain one layer of metal M sandwiched between two layers of X, leading to novel characteristics for the IF nanotubes. This, in turn, affects their tensile strength and electronic properties.[3,4]

IF nanotubes have usually been produced from gaseous H_2S and metal oxides.[16–19] Early experiments generated mainly small tubes and nanoparticles, whereas recent investigations have successfully produced significant quantities of long tubes (microtubes).[19–20] Based on direct TEM observations, an oxide–sulfide conversion process has been proposed by Tenne *et al.* to account for IF nanoparticle (and nanotube) formation.[18] Using TEM dark-field imaging techniques, Margulis *et al.* studied the chirality of IF nanotubes prepared from WO_3 and H_2S in a H_2 atmosphere.[21] Sloan *et al.* examined IF nanotubes containing encapsulated WO_{3-x} phase defects and assessed their effects on the WS_2 tube walls, by high resolution transmission electron microscopy (HRTEM) and ED.[22] Wrapped nanotubes, ribbons and defective WS_2 structures have also been described by Remskar *et al.*[23] Preliminary studies on potential applications have revealed the extraordinary wear-resistant behaviour and optical properties of the IF nanotubes.[24] A single WS_2 nanotube has been used recently as a scanning tunnelling microscope probe.[25]

In a previous study, we created highly pure WS_2 nanotubes by heating WO_x ($x \cong 2.7$) nanorods or needles in the presence of gaseous H_2S.[26] In this paper, we present an in-depth morphological and structural analysis of these WS_2 nanotubes, in comparison with CNTs. Our results suggest that an alternative mechanism, as regards the oxide–sulfide conversion model,[18] may be responsible for extended IF nanotube growth.

2. Experimental

The WS_2 nanotubes were prepared by reacting WO_x nanorods with gaseous H_2S at *ca.* 1100 °C as previously described.[26] The resulting WS_2 nanotubes were dispersed ultrasonically in acetone for 5 min, then transferred for TEM measurements to a Cu grid coated with a holey carbon film. The following equipment was employed, as appropriate: SEM (Leo 5420, 10–20 kV), HRTEM (CM200, JEM-200, 2000, operating at 200 kV; and JEM-4000 operating at 400 kV); energy dispersive X-ray (EDX, element ≥ B) and a VG HB501 scanning transmission electron microscope (STEM) for elemental analysis.

3. Results and discussion

3.1 Phases and chemical composition

An SEM image (Fig. 1) shows that the WS_2 nanotubes prepared in this study are long (*ca.* >100 nm) and relatively free of nanoparticles (*ca.* <30%). They differ from nanotubes made from commercial WO_3 particles in that they are relatively short. Some of the nanotubes exhibited polygonal cross-

 DOI: 10.1039/b004433o

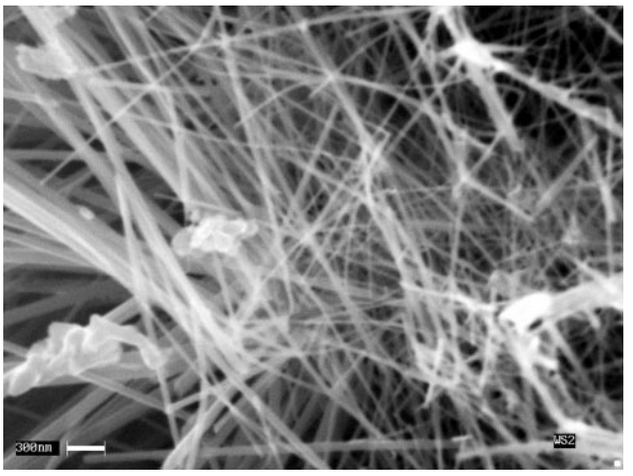

Fig. 1 SEM image of long nanotubes.

sections, possibly because the *in-situ* grown WO_x nanorods possess this feature.[27] However, SEM measurements failed to identify a typical cross-section.

XRD was employed to characterise the general phases of the sample examined by SEM, and compared with commercial WS_2 particles (Aldrich Co., >99.9% pure and $\leqslant 2\,\mu m$ diameter) and simulated WS_2 single crystals ($100 \times 20 \times 20$ nm), Fig. 2. Our results revealed that WS_2 predominated, and was accompanied by a small amount of W and minute quantities of WO_x ($x = 2$–3) complex. The WS_2 phase exhibits an interlayer distance of 0.62 nm, which is slightly larger than those distances found in commercial and simulated WS_2 particles. This result is in accord with previous XRD studies on WS_2 and MoS_2 nanotubes.[17,28] The average WS_2 nanotube diameter (*ca.* 30 nm) was calculated using the Debye–Scherrer formula. The approximate number of layers (*ca.* 10–20) within a nanotube was estimated by carefully examining the (002) peak profile and its half-width. From a comparison with the two accompanying reference profiles for WS_2 powders, we found that the (002) peak intensity, arising from successive S–W–S sandwiches, tends to be quite sharp. However, the higher angle peaks, *e.g.* (004), (006), (008) and (0012), governed by the long periodic layers of the crystal, are obviously broadened and weak, indicating a poorer long distance order within the nanotube. This phenomenon agrees well with the ED study, in which the (004), or higher diffraction spots, were barely observable.[16] The asymmetric broadening and increased intensity of the (100) and (101) peaks (Fig. 2),

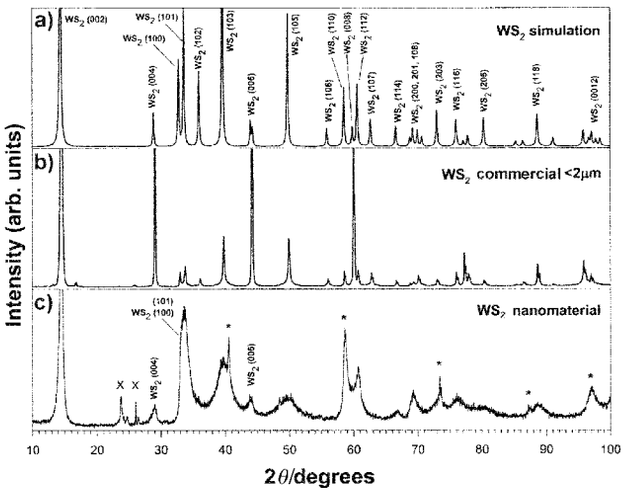

Fig. 2 X-Ray diffraction patterns of WS_2 nanomaterials, accompanied by simulated (a) and commercial WS_2 powders (b). Nanomaterials include nanotubes, nanoparticles and WO_x ($x = 2$–3) and W residues.

determined by the 3-D atomic positions within the IF nanotubes, might be caused by network (cylinder) rotation along the tube axis, analogous to the situation in helical carbon nanotubes.[1] The (100) and (101) peak intensities of the commercial WS_2 are very weak by comparison with the simulated nano-crystals and actual nanotubes. It is possible that the elongated structures of the nanotubes and the simulated nano-crystals ($100 \times 20 \times 20$ nm), by comparison with commercial particles ($2 \times 2 \times 2\,\mu m$), are responsible for the significantly higher intensities. Meanwhile, defective structures and dislocations can also lead to broadened peaks. It is noteworthy that the (004) peak intensity may overlap with complex WO_x phases present in the sample. Furthermore, such complex phases must also contribute to other peaks. To the best of our knowledge, based on a previous XRD study of WO_x nanorods,[27] we can only identify the two obvious peaks (marked with an X in Fig. 2), which probably correspond to the $W_{18}O_{49}$ phase. The other peaks are too weak to be indexed. This analysis agrees with Feldman *et al.*'s conjecture that IF nanotube growth begins with the reduced WO_x phase, particularly $W_{18}O_{49}$.[17] Because of the numerous intermediate phases for WO_x, it is difficult, from XRD measurements, to identify precisely one particular WO_x phase. HRTEM and ED examinations in this case provide a better understanding of the WO_x encapsulated phases.

In the TEM, the samples were found to consist of many different phases and particles including flat WS_2 sheets, rolled up WS_2 sheets, long thin rods of WS_2 and WS_2 nanotubes. The WS_2 rods looked similar to the WS_2 nanotubes when viewed down the WS_2 [0001] direction. Their edges were coated in a thin layer of WS_2 oriented with [0001] perpendicular to the beam and pointing away from the main crystal. True WS_2 nanotubes were distinguishable by their thicker walls and hollow centres.

EDX measurements verified the chemical composition of a single WS_2 nanotube (Fig. 3a). For hollow tubes, only W and S were detected. However, for nanotubes containing encapsulated material, O was found together with W and S (Fig. 3b). Different spots spanning an isolated nanotube were subjected to EELS examination using a VG HB 501 STEM. Figs. 4a and 5a are dark field images showing the area analysed. The EELS spectra arising from an energy loss of the S–K edge are shown separately in Figs. 4b and 5b. For a filled nanotube, EELS results confirmed the existence of a lower S content, arising from the WS_2 shells, within the filled region (Figs. 4a and 4b). This result is most likely to be due to the presence of WO_x phases. Fig. 5b reveals that there is almost no noticeable difference between the outer and inner tube walls, indicating uniformity as regards S distribution within the various nanotube walls. In Fig. 5, the slightly lower concentration at the outer edge (spot 7) could be due to S vacancies at the tube edge. A recent study using atomic force microscopy (AFM) has revealed S vacancies located at the edges of single-layered MoS_2 clusters.[29] This phenomenon could also occur in WS_2. This type of vacancy is expected to lead to unstable and/or defective structures, in the outer layers of a tube. The above analysis demonstrates that our samples consist of WS_2 nanotubes, with some encapsulated WO_x. The compositions of the hollow nanotubes are generally uniform.

3.2 Morphology characterisation

Under HRTEM examination, a typical well-grown nanotube is rather straight (Fig. 6a). Its WS_2 (S–W–S) layers, separated by 0.62 nm, are evenly distributed on either side (*ca.* 14 layers in this case). This tube has been shown to be of circular cross-section, by rotating the sample holder along the tube axis during the observation. Its inner core is hollow, straight and uniform (*ca.* 5 nm diameter). CNTs created by graphite arc-discharge techniques show similar structural uniformity.[1]

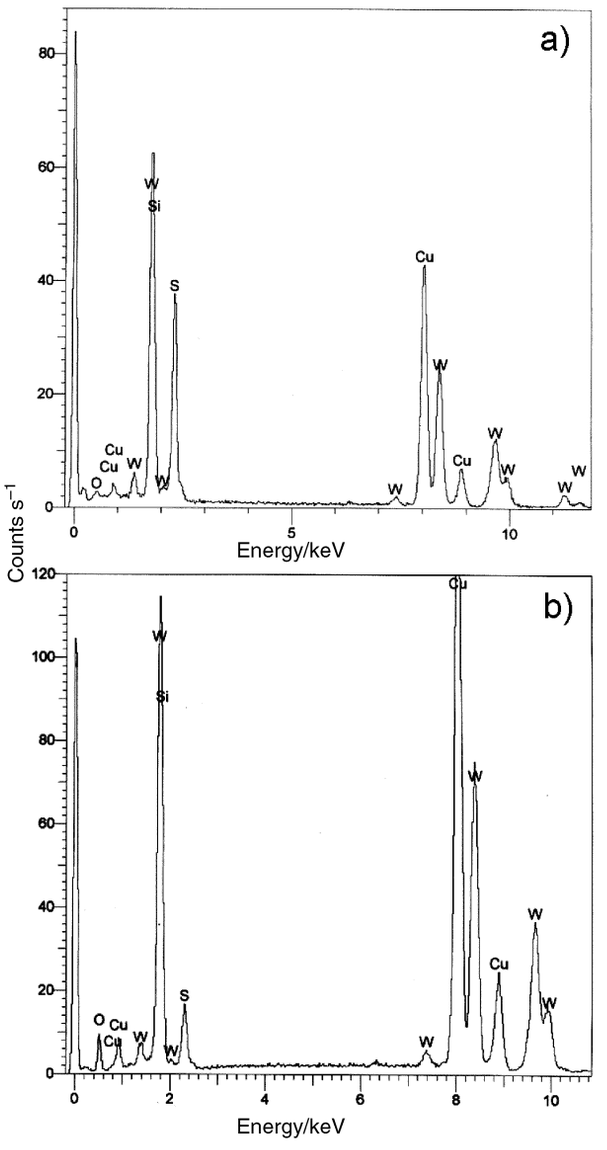

Fig. 3 EDX profiles: a) hollow tube, b) WO_x encapsulating tube. The Cu signals arise from the TEM support grid.

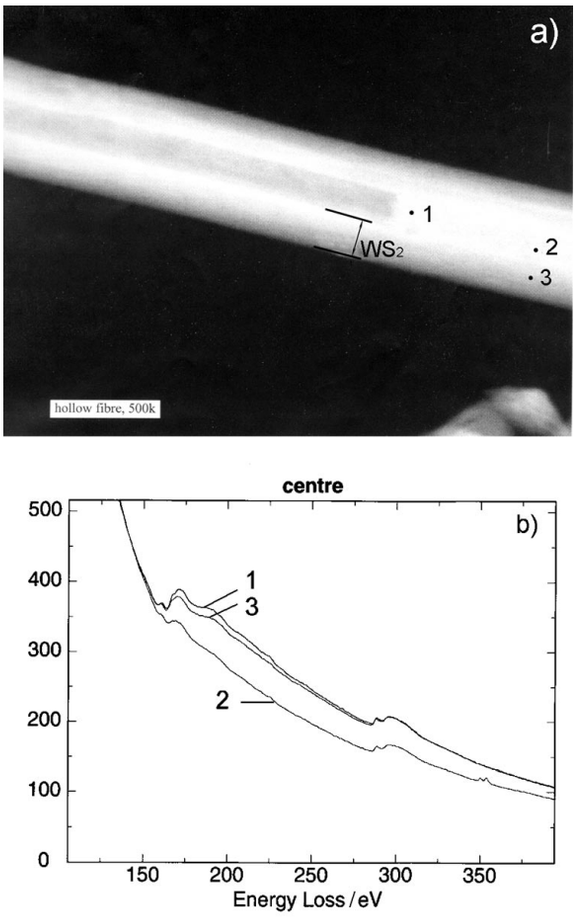

Fig. 4 EELS analysis: a) annular dark field image of a partly filled WS_2 tube (tube wall marked). Measurements were taken from spots 1, 2 and 3, which represent the edge and centre of the filling phase and the tube wall; b) EELS spectrum showing the S–L2 edge at 165 eV from the three areas 1, 2 and 3. The S content is lower at the centre (spot 2). The C–K edge at *ca.* 285 eV may arise from carbon contamination because of the use of acetone during preparation of the TEM sample.

The nanotube tips exhibit various structures (Fig. 6b–d), which are quite different from those of CNTs. However, open-ended exceptions have often been observed during TEM examinations (Fig. 7a–d). For well-grown CNTs, six 5-membered rings have been introduced, as in the half fullerene cage, to account for positive curvature and nanotube closure.[30] As for IF nanotubes, we believe that the closure could be far more complicated. To date, the possibility of 3-, 4- and 8-membered rings causing positive curvature in nanotubes has been discussed.[22,31] In our account, we have used molecular mechanics computer simulations to successfully establish two types of IF nanotube cap, by introducing square-like and octagonal-like defects associated with zigzag and armchair nanotubes, respectively. (To simplify the process, only a single layer MX_2 nanotube model was considered, even though a single-layered IF structure has yet to be observed). Both types of defect are most likely to produce flat caps provided hexagons are involved (Figs. 8a and b), whereas octagonal defects (involving 8-membered rings) tend to generate negative curvature. Topologically, these two types of defective structure could equally well be formed, thus leading to either zigzag or armchair tubes. However, our observations revealed that flat WS_2 nanotube caps dominated, and our ED analysis (section 3.4) revealed the predominance of armchair tubes, indicating that octagonal defects are probably favoured.

The open-tipped nanotubes can be classified in several ways: a) flat open-ended (Fig. 7a); b) outside open-ended cone (Fig. 7b); c) inside open-ended cone (Fig. 7c); and d) 'pseudo' closed ended with flat layers lying on the opening area in various ways (Fig. 7d). The tubes differ from the CNTs, which are usually completely sealed in order to remove dangling bonds by pentagonal dislocations. This may not be surprising as perfect closure of a single graphite sheet is significantly easier to achieve than is likely to be the case for a S–W–S sandwich, which may only be possible for a few specific topologies. These observations imply that: 1) IF nanostructures may not 'self-seal' and, 2) an alternative growth mechanism may result in well-shaped open-tipped nanotubes. A recent AFM study of the behaviour of MoS_2 clusters on a gold surface confirmed that S vacancies exist at the edge of the crystal.[29] Therefore one would not expect self-sealing to be generally feasible for IF nanotubes. In this context, the oxide-to-sulfide conversion mechanism proposed by Tenne *et al.* may apply to normal (close-capped) IF nanotubes.[17] Because this conversion of WO_x nanorods should occur evenly at the rod tips and around the rod bodies, the WO_x should be totally enclosed by the growing WS_2 layers and close-tipped nanotubes should result. The outcome is therefore akin to CNTs, exhibiting fullerene-like cage structures (hence the term IF nanotubes). This phenomenon has been studied experimentally by HRTEM.[17] However, for abnormal tubes (with open-tips, we

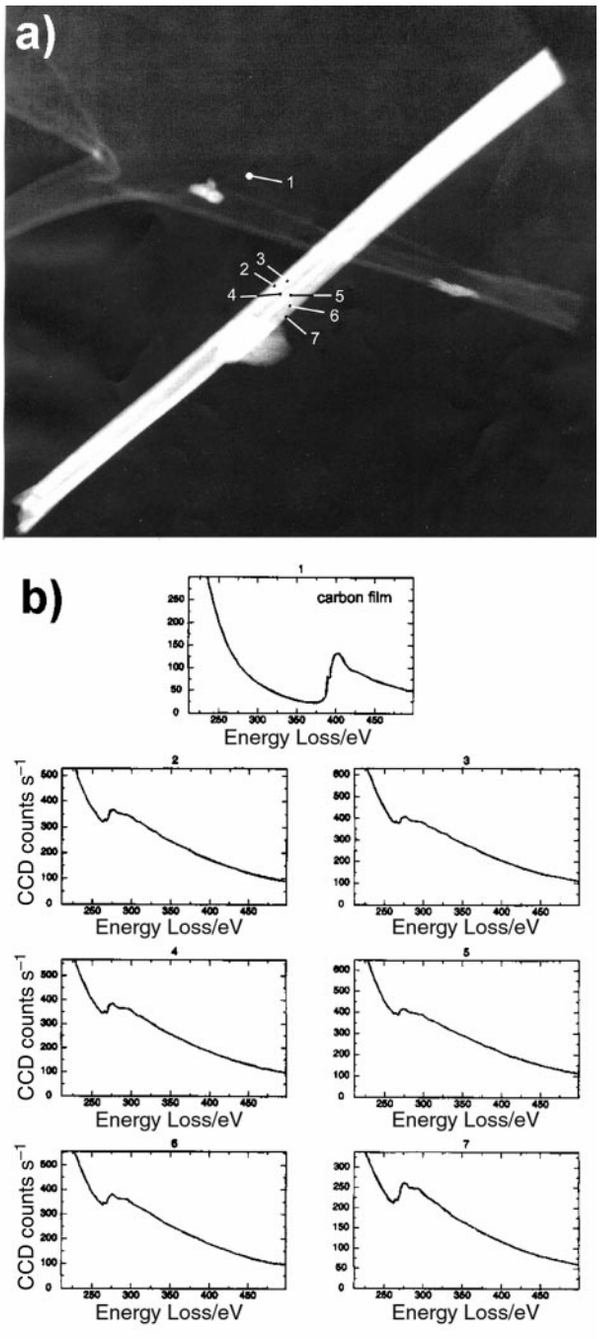

Fig. 5 EELS analysis: a) dark field image of a nanotube, showing the areas where EELS spectra were acquired. The results are shown in b). Spot 1 corresponds to the carbon film.

continue using the term 'IF nanotube'), this conversion mechanism is unlikely to apply (*vide infra*).

3.3 Structural defects

Under specific conditions, CNTs, produced by chemical vapour deposition are often coiled, exhibiting various multilayer dislocations and poorly graphitised domains. For IF nanotubes, ribbons and bundles have also been produced using a vapour transport method.[23] In this paper, we also describe WS_2 nanotubes containing significant defective structures. In a few cases, we found that the inner core diameter of a WS_2 nanotube had changed (Figs. 9a and 9b), so that in some regions, it appeared to be a fibre (or rod) rather than a tube. Fig. 9b suggests that the number of layers at different points (arrowed) is different. Therefore, it is unlikely that the fibre (rod) is formed by collapse of the hollow core due to external

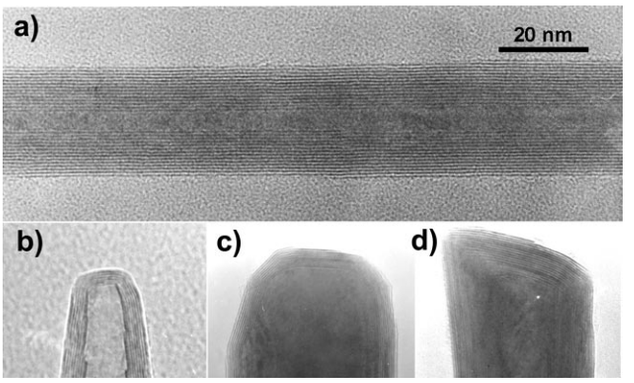

Fig. 6 HRTEM images: a) a typical well-grown WS_2 nanotube of *ca.* 14 layers, with hollow core and uniform layer separation; b–d) various closed tips, possibly containing square and octagonal defects.

(*e.g.* mechanical) forces. Since our starting materials were WO_x nanorods,[27] we suggest that this defective structure may be due to an original WO_x nanorod with variable diameter.

The most interesting and informative 'closed' structure (Fig. 10) differs significantly from those structures observed for CNTs. The inner core of the closed tube is hollow, and the inner layers terminate sequentially, in contrast to CNTs whose layers are gradually closed, albeit with varied spacing.[32] This open inner-layered structure has rarely been reported for pure CNTs, but occurs quite frequently for metal-filled CNTs.[33] The layer numbers (*i.e.* the wall thickness) vary on both sides. For a partly filled WS_2 nanotube, Sloan *et al.* have studied the occurrence of WO_x vacancies and concluded that, during the oxide-to-sulfide conversion, vacancies form resulting in a hollow structure.[22] This nanotube (Fig. 10a) has been converted completely, however for some reason the position of the 'vacancy' (*i. e.* the hollow core) is uneven (*e.g.* temperature difference or the H_2S penetration rate may lead to different conversion rates). As a consequence, uneven-walled nanotubes form, which may provide further evidence in support of the conversion mechanism proposed by Tenne *et al.*[18] Taking into account the entire process, particularly when the transformation is almost complete, it is not yet clear why many IF nanotubes are highly symmetrical, as in Fig. 6a.

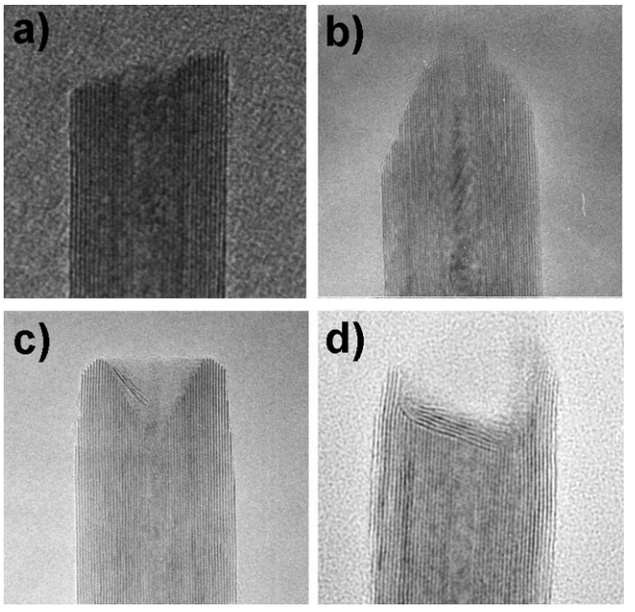

Fig. 7 HRTEM images of the open-ended tubes, which can be classified as: a) open-ended with flattened layers; b) open-ended with inside longer layers; c) open-ended with outside longer layers; and d) 'pseudo' closed tip with flat layers lying on the opening areas, of which b) and c) were observed for IF MoS_2 samples.

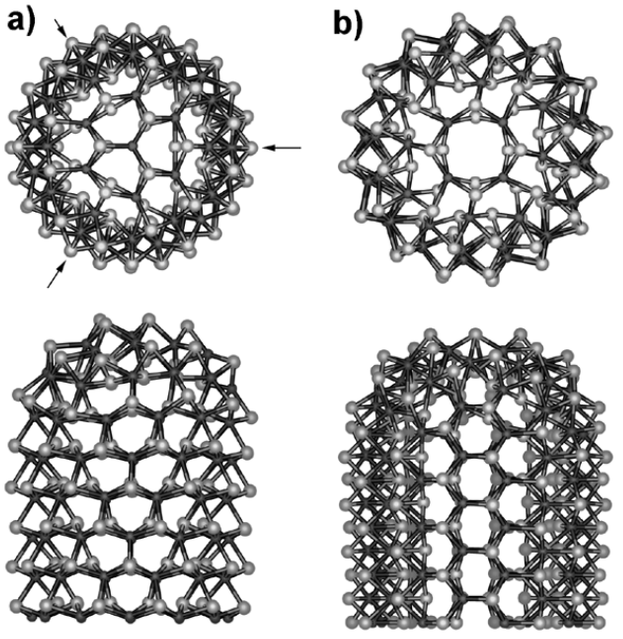

Fig. 8 Models of MX2 nanotubes and associated tip structures: a) zigzag tube contains 3 square defects at the tip (arrowed); b) armchair tube contains an octagonal defect at the centre of the tip.

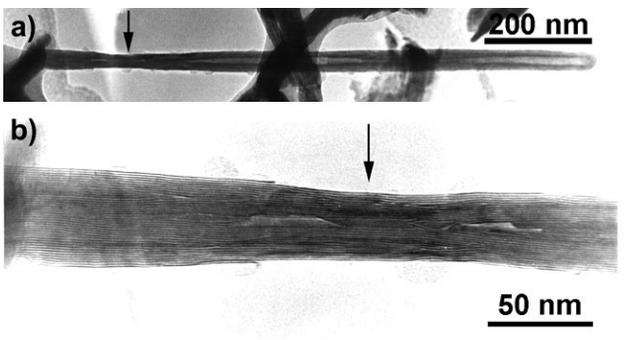

Fig. 9 TEM images: a) a very long nanotube whose diameter varies along its length; b) an enlargement of the arrowed area in a), note the change in the number of the layers (arrowed).

Layer defects have often been observed in WO_x containing nanotubes. Fig. 11a shows a type of plane defect (arrowed) which appears to be a bifurcation point for two layers. This could arise from the inner encapsulated phase. From its HRTEM image, the crystallographic shear (CS) feature of the inner WO_x phase appears to be discrete. Hence, these original plane defects may transform so as to generate WS_2 layers. This effect has been investigated comprehensively by Sloan *et al.*[22] Meanwhile, Remskar's study has revealed that each WS_2 layer has to satisfy the stacking order and orientation relationship with respect to the previous layers, and the strain involved can be relaxed by forming edge dislocations.[19] In our samples, we found that the defects (or dislocations) tended to occur near the edges, probably because the outer cylinders are subject to less stress than are the inner shells. This internal stress, inherent in concentric cylinders, should tighten and stabilise the inner shells, so that outer layer deformation should be easier. Another reason may be that the lower S content at the tube outer edge (Fig. 5) leads to unstable structures and to defects. In Fig. 11b, a blister-like defect is present. This onset of positive curvature may be due to a tiny attachment (*e.g.* a WO_x particle) to the original WO_x nanorod. In our previous WO_x nanorod study, we observed a very small quantity of tiny particles attached to the nanorod surface.[27] Such attached growth for IF nanotubes has been reported by Remskar *et al.*[34]

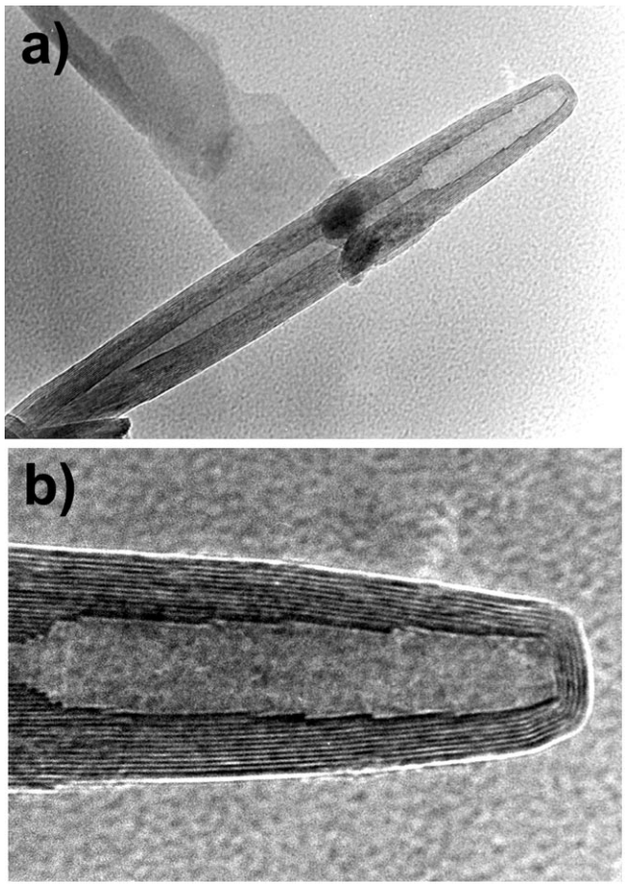

Fig. 10 TEM images of a nanotube: a) inner layers remaining open; tube wall with various layers; b) enlargement.

3.4 Nanotube chirality

Concentric cylinders, constituting CNTs, exhibit various chiralities and may also be a feature of IF nanotubes. It has been pointed out that the electronic properties of CNTs depend on the tube structures: they can be either metallic or semiconducting, depending upon their helicity.[3,4] The structure–property relationships for IF nanotubes have only recently been studied.[35,36] ED, AFM and dark field imaging techniques have been used to monitor CNT helicity, but only a few IF nanotubes have been monitored in this way. Because of the complexity of the actual curved and rotated tubes, it is not easy to account for the observed diffraction patterns exhibited by CNTs. Iijima's work was illustrated by a CNT helix.[32] Zhang *et al.*'s study provided a comprehensive method for assessing the complicated diffraction patterns of CNTs.[37] In the present account, and with the assistance of computer simulations (Fig. 12), we were able to interpret the ED patterns

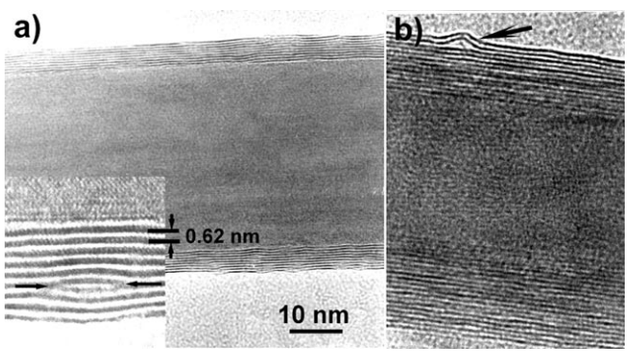

Fig. 11 HRTEM images of WO_x encapsulating WS_2 tubes: a) many layer defects were observed. The insert enlargement shows a bifurcation defect; b) a blister was formed at the outer shells (arrowed).

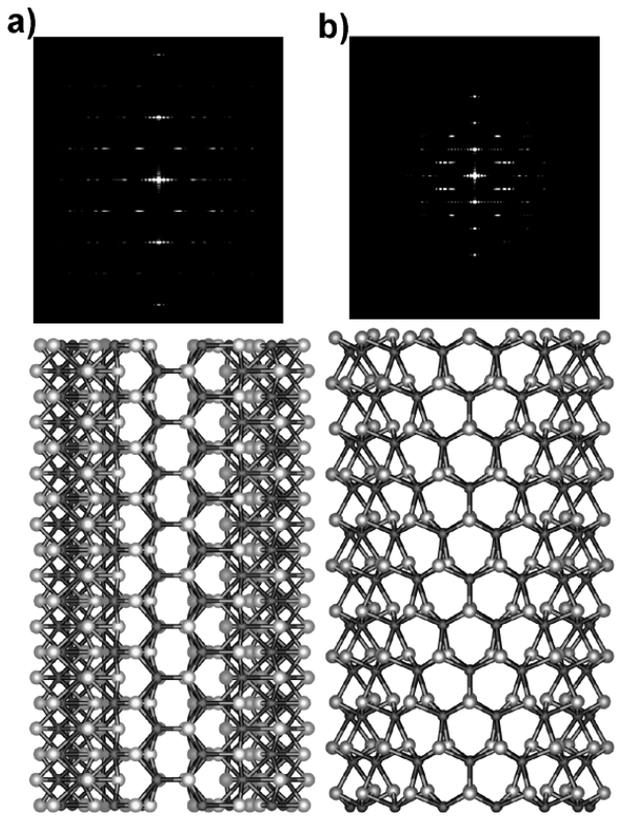

Fig. 12 Simulated single-layered MX_2 tubes: a) armchair tube (8-8), and b) zigzag tube (14-0). The ED patterns are inserted in the cross-sections.

of IF nanotubes. Fig. 12 illustrates single-layered (non-helical) nanotubes. Armchair (8-8) and zigzag (14-0) tubes are present, together with their resulting simulated ED patterns along the $\langle 001 \rangle$ direction (perpendicular to the tube axis). The unit cell structure of a nanotube is obtained by mapping the flat triple MX_2 layer on to the surface of a cylinder. This unit cell is then relaxed using a force field approach with the conjugate gradient method, in order to optimise the bond lengths and angles. Further optimisation might be achieved using the density functional tight binding method.[36] The simulated ED patterns were obtained using the diffraction and HRTEM moduli of the CERIUS^2 program, developed by Molecular Simulations Inc. These simulations provide the basic ED information for the two possible non-helical tubes. It is apparent that the difference between the armchair and zigzag patterns lies in the fact that their (100) and (110) planes (ignoring curvature) exhibit different angles subtended at the tube axis. The tube axis can be recognised from its typical (002) spots. We have examined many isolated WS_2 nanotubes, and recorded a range of typical diffraction patterns as shown in Fig. 13.

We observed that nearly half of the WS_2 nanotubes exhibited patterns consistent with helicity (Fig. 13a). The two prominent (002) spots and dot-rings (Fig. 13a) characterise chirality. (Detailed information about the chirality of WS_2 nanotubes has been discussed in ref. 21). About half of the tubes exhibited non-helical patterns, as indicated by the diffraction spots in Figs. 13b and 13c. It is noteworthy that the simulated patterns do not contain the (002) diffraction (the two inner symmetric bar-like dots in Fig. 13) because the simulations cover only a single-layered tube. When compared with the simulations, the main feature of the observed patterns (brighter individual diffraction dots) match very well with the pattern obtained for the armchair structure. The brighter dot (top right) in the first dot-ring (Fig. 13c), corresponds to the (100) planes and the brighter dot on the top in the second dot-ring corresponds to (110) planes of the WS_2 crystals. The (less bright) diffraction

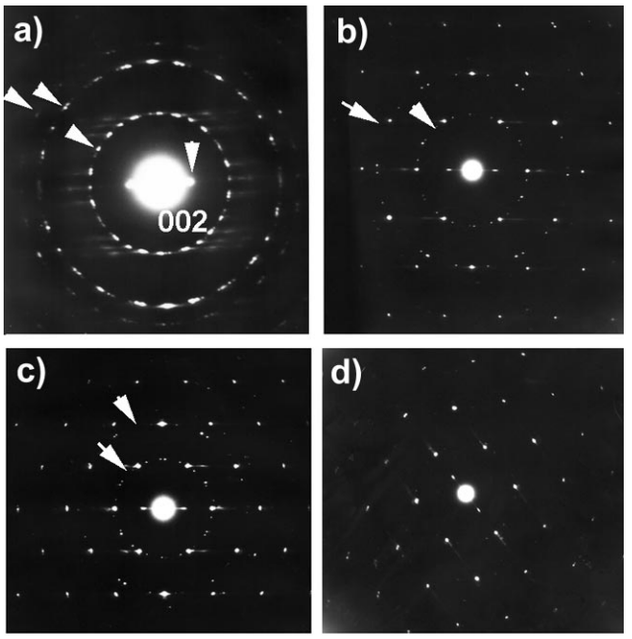

Fig. 13 ED patterns revealing the various tube chiralities (electron beams vertical to the tube axis): a) a helix tube; b) and c) armchair tubes with modest layer rotations, indicated by diffraction rings (arrowed); d) armchair tube.

rings (arrowed) reveal that some of the cylinders have rotated. For example, if the layer distance of a tube remains constant, the (002) dot will not change. This is also true when some of its layers rotate slightly along the tube axis. However, after such rotation, the (100) planes may show various diffraction dots with the same distances, leading to a dot-ring. Zhang *et al.* have pointed out that it is possible to measure the rotation angle, however a high degree of technical accuracy is required.[37] After examining a considerable number of ED patterns (*ca.* 40), we conclude that all non-chiral patterns are consistent with armchair tubes (Fig. 13d) and none with zigzag structures. Similar results are evident in ED patterns, recorded for WS_2 nanotubes, prepared by others using different routes.[16,23] These results also agree with our observations that flat caps arise from octahedral defects contained in armchair tubes. This result is different from that observed for CNTs, in which both zigzag and armchair tubes are commonly observed. The results suggest that the armchair configuration is the favoured structure for WS_2 nanotubes. Further research along these lines is in progress.

3.5 Growth mechanism

Tenne *et al.* proposed an oxide–sulfide template conversion model, based on TEM evidence, in order to account for IF formation.[17] Sloan *et al.* extended this mechanistic concept and discussed how the conversion might occur from the crystallographic viewpoint.[22] The main feature of this model is that the outer IF layers form first from the oxide. Growth then proceeds on the inner face, a hollow core remaining as a result of structural differences between oxide and sulfide. Therefore, closed nanotubes, particularly nanoparticles, depend upon the initial oxide, which is a key feature of this mechanism. In our study, this model can account for the observations, *e.g.* polygonal WS_2 cross-sections that originate from the polygonal WO_x nanorods, different nanotube diameters resulting from defective initial nanorods, and the significantly longer nanotubes which are a feature of this work. However, for some structures (section 3.2), such as open-tipped tubes, this model appears to be untenable. We suggest that these open-tips may result from a continuous growth on the part of certain nanotubes.

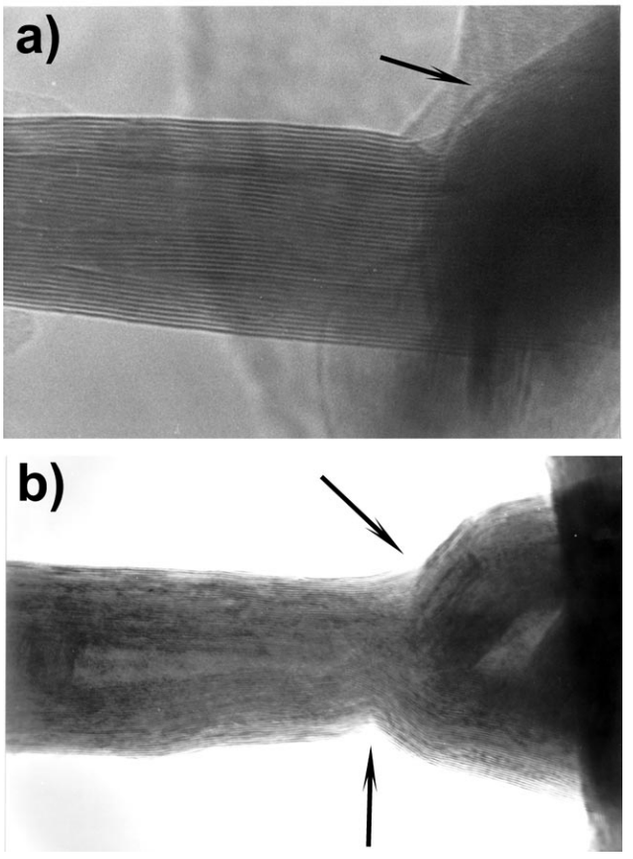

Fig. 14 HRTEM images: a) a tube/fibre attached to dark powders, the layer continuity can be seen (arrowed); b) a nanotube attached to a nanoparticle, only the outer layers are well formed in the neck area (arrowed).

During HRTEM investigations, we observed in a few cases that one end of a nanotube was rooted in a dark area consisting of a densely-packed WS_2–WO_x mixture, according to EDX measurements. By examining the fringes, we can detect layer continuity (Fig. 14a, arrowed), which indicates that this tube (or fibre) may be growing out of this area. It is noteworthy that our experimental method is based on a simple heating process, the average temperature being *ca.* 1100 °C (optical pyrometry). In some regions, the temperature might well be higher than the average, so that WS_2 vapour may be present in the reactor. As long as a WS_2 nucleus forms, continuous growth is possible as a result of deposition, involving atomic spiral growth which occurs in the vapour transport process.[19,20] In practice, the open-tip facilitates easier H_2S penetration of the tube. Hence, it is possible that continuous growth occurs at both ends (even if only one end is rooted within the starting materials). This proposal can account for the formation of open-tipped tubes. Given these special circumstances, such a growth may be similar to that of CNTs, but without involvement of catalyst.[38] For other ceramic nanotubes (*e.g.* VO_x), open-tips are often observed.[13,14] We believe that this feature can eventually lead to large nanotubes, as well as microtubes,[23,39] provided that the growth conditions are maintained.

It is conceivable that a nanotube may coalesce with an adjacent nanoparticle to form a new structure, as a result of continuous growth. Such a feature has been observed (Fig. 14b). The atomic layers, forming the neck (arrowed), exhibit good continuity between the tube and the particle, particularly in the outer shells. In a previous report, nanotube coalescence was also explored, in order to obtain evidence for continuous growth.[34] This conjecture was also supported by Tenne's study of small nanotubes, the lengths of which can be extended.[16] However, it is not yet clear how the nuclei are formed.

4. Summary

We have studied the morphological and structural features of WS_2 nanotubes, and compared them with CNTs, using HRTEM, ED, EDX, EELS and XRD together with computer simulations. The results show that these IF nanotubes differ from CNTs, in that tube tips are often open. Both even and uneven walled tubes are observed. The composition within the tubes is fairly uniform, except for the edge layers which may contain slightly lower S levels. Defects are often observed in the outer shells. Octagonal and square defects appear to be involved in forming tube caps. ED examinations reveal that *ca.* half of the WS_2 nanotubes are chiral, however significant amounts of (*ca.* half) non-helical nanotubes are often found. Interestingly, all non-helical nanotubes appear to be of the armchair-type. An alternative growth mechanism has been proposed to account for the extended IF nanotube growth.

Acknowledgements

We thank the Royal Society, the JFCC, Conacyt-Mexico and DGAPA-UNAM (HT), and the EPSRC, for financial support. We are grateful to J. Thorpe and D. Randall (Sussex) for assistance with TEM and SEM facilities.

References

1 S. Iijima, *Nature*, 1991, **354**, 56.
2 S. Sawada and N. Hamada, *Solid State Commun.*, 1992, **83**, 917.
3 J. W. Mintmire, B. I. Dunlap and C. T. White, *Phys. Rev. Lett.*, 1992, **68**, 631.
4 Y. Saito, K. Hamaguchi, K. Hata, K. Uchita, Y. Tasaka, F. Ikazaki, M. Yamura, A. Kasuya and Y. Nishina, *Nature*, 1997, **389**, 554.
5 T. Guo, P. Nikolaev, A. G. Rinzler, D. Tomanek, D. T. Colbert and R. E. Smalley, *J. Phys. Chem.*, 1995, **99**, 10694.
6 M. Terrones, N. Grobert, J. Olivares, J. P. Zhang, H. Terrones, K. Kordatos, W. K. Hsu, J. P. Hare, P. D. Townsend, K. Prassides, A. K. Cheetham, H. W. Kroto and D. R. M. Walton, *Nature*, 1997, **388**, 52.
7 W. Z. Li, S. S. Xie, L. X. Qian, B. H. Chang, B. S. Zou, W. Y. Zhou, R. A. Zhao and G. Wang, *Science*, 1996, **274**, 1701.
8 Z. F. Ren, Z. P. Huang, J. W. Xu, J. H. Wang, P. Bush, M. P. Siegal and P. N. Provencio, *Science*, 1998, **282**, 1105.
9 S. S. Fan, M. G. Chapline, N. R. Franklin, T. W. Tombler, A. M. Cassell and H. J. Dai, *Science*, 1999, **283**, 512.
10 N. G. Chopra, R. J. Luyken, K. Cherrey, V. H. Crespi, M. L. Cohen, S. G. Louie and A. Zettl, *Science*, 1995, **269**, 966.
11 O. Stephan, P. M. Ajayan, C. Colliex, P. Redlich, J. M. Lambert, P. Bernier and P. Lefin, *Science*, 1994, **266**, 1683.
12 M. Terrones, A. M. Benito, C. Manteca-Diego, W. K. Hsu, O. I. Osman, J. P. Hare, D. G. Reid, H. Terrones, A. K. Cheetham, K. Prassides, H. W. Kroto and D. R. M. Walton, *Chem. Phys. Lett.*, 1996, **257**, 576.
13 F. Krumeich, H. J. Muhr, M. Niederberger, F. Bieri, B. Schnyder and R. Nesper, *J. Am. Chem. Soc.*, 1999, **121**, 8324.
14 T. Kasuga, M. Hiramatsu, A. Hoson, T. Sekino and K. Niihara, *Adv. Mater.*, 1999, **11**, 1307.
15 M. Zhang, Y. Bando and K. Wada, *J. Mater. Res.*, 2000, **15**, 387.
16 R. Tenne, L. Margulis, M. Genut and G. Hodes, *Nature*, 1992, **360**, 444.
17 Y. Feldman, G. L. Frey, M. Homyonfer, V. Lyakhovitskaya, L. Margulis, H. Cohen, G. Hodes, J. L. Hutchison and R. Tenne, *J. Am. Chem. Soc.*, 1996, **118**, 5362.
18 M. Homyonfer, B. Alperson, Y. Rosenberg, L. Sapir, S. R. Cohen, G. Hodes and R. Tenne, *J. Am. Chem. Soc.*, 1997, **119**, 2693.
19 M. Remskar, Z. Skraba, C. Ballif, R. Sanjines and F. Levy, *Surf. Sci.*, 1999, **435**, 637.
20 A. Rothschild, G. L. Frey, M. Homyonfer, R. Tenne and M. Rappapport, *Mater. Res. Innov.*, 1999, **3**, 145.
21 L. Margulis, P. Dluzewski, Y. Feldman and R. Tenne, *J. Microsc. (Oxford)*, 1996, **181**, 68.

22 J. Sloan, J. L. Hutchison, R. Tenne, Y. Feldman, T. Tsirlina and M. Homyonfer, *J. Solid State Chem.*, 1999, **144**, 100.
23 M. Remskar, Z. Skraba, M. Regula, C. Ballif, R. Sanjines and F. Levy, *Adv. Mater.*, 1998, **10**, 246.
24 L. Rapoport, Y. Feldman, M. Homyonfer, H. Cohen, J. Sloan, J. L. Hutchison and R. Tenne, *Wear*, 1999, **229**, 975.
25 A. Rothschild, S. R. Cohen and R. Tenne, *Appl. Phys. Lett.*, 1999, **75**, 4025.
26 Y. Q. Zhu, W. K. Hsu, N. Grobert, B. H. Chang, M. Terrones, H. Terrones, H. W. Kroto, D. R. M. Walton and B. Q. Wei, *Chem. Mater.*, 2000, **12**, 1190.
27 Y. Q. Zhu, W. B. Hu, W. K. Hsu, M. Terrones, N. Grobert, H. Terrones, H. W. Kroto and D. R. M. Walton, *Chem. Phys. Lett.*, 1999, **309**, 327.
28 Y. Feldman, E. Wasserman, D. J. Srolovitz and R. Tenne, *Science*, 1995, **267**, 222.
29 S. Helveg, J. V. Lauritsen, E. Laegsgaard, I. Stensgaard, J. K. Norskov, B. S. Clausen, H. Topsoe and F. Besenbacher, *Phys. Rev. Lett.*, 2000, **84**, 951.
30 S. Iijima, *Mater. Res. Bull.*, 1994, **19**, 43.
31 M. Terrones, W. K. Hsu, H. Terrones, J. P. Zhang, S. Ramos, J. P. Hare, R. Castillo, K. Prassides, A. K. Cheetham, H. W. Kroto and D. R. M. Walton, *Chem. Phys. Lett.*, 1996, **259**, 568.
32 S. Iijima and T. Ichihashi, *Nature*, 1993, **363**, 603.
33 N. Grobert, M. Terrones, A. J. Osborne, H. Terrones, W. K. Hsu, S. Trasobares, Y. Q. Zhu, J. P. Hare, H. W. Kroto and D. R. M. Walton, *Appl. Phys. A.*, 1998, **67**, 595.
34 M. Remskar, Z. Skraba, R. Sanjines and F. Levy, *Appl. Phys. Lett.*, 1999, **74**, 3633.
35 G. Seifert, H. Terrones, M. Terrones, G. Jungnickel and T. Frauenheim, *Solid State Commun.*, 2000, **114**, 245.
36 G. Seifert, H. Terrones, M. Terrones, G. Jungnickel and T. Frauenheim, *Phys. Rev. Lett.*, 2000, **85**, 146.
37 X. F. Zhang, X. B. Zhang, G. V. Tendeloo, S. Amelinckx, M. O. Beeck and J. V. Landuyt, *J. Cryst. Growth*, 1993, **130**, 368.
38 Z. W. Pan, S. S. Xie, B. H. Chang, L. F. Sun, W. Y. Zhou and G. Wang, *Chem. Phys. Lett.*, 1999, **299**, 97.
39 M. Remskar, Z. Skraba, F. Cleton, R. Sanjines and F. Levy, *Appl. Phys. Lett.*, 1996, **69**, 351.